metals

MDPI

Article

Effect of Cobalt on the Microstructure of Fe-B-Sn Amorphous Metallic Alloys

Daniel G. Grey [1], Martin Cesnek [2], Marek Bujdoš [3] and Marcel B. Miglierini [1,2,*]

[1] Institute of Nuclear and Physical Engineering, Faculty of Electrical Engineering and Information Technology, Slovak University of Technology, Ilkovičova 3, 841 04 Bratislava, Slovakia; daniel.grey@stuba.sk
[2] Department of Nuclear Reactors, Faculty of Nuclear Science and Physical Engineering, Czech Technical University in Prague, V Holešovičkách 2, 180 00 Prague, Czech Republic; martin.cesnek@fjfi.cvut.cz
[3] Institute of Laboratory Research on Geomaterials, Faculty of Natural Sciences, Comenius University in Bratislava, Mlynská dolina, Ilkovičova 6, 842 15 Bratislava, Slovakia; marek.bujdos@uniba.sk
* Correspondence: marcel.miglierini@stuba.sk

Abstract: $Fe_{78}B_{15}Sn_7$ and $(Fe_3Co_1)_{78}B_{15}Sn_7$ amorphous metallic alloys were prepared using the method of planar flow casting. The amorphous nature of ribbons containing 7 at. % Sn was verified by X-ray diffraction. The resulting chemical composition was checked by flame atomic absorption spectroscopy and by mass spectrometry with inductively coupled plasma. The microstructure of the as-quenched metallic glasses was investigated by 57-Fe and 119-Sn Mössbauer spectrometry. The experiments were performed with transmission geometry at 300 K, 100 K, and 4.2 K, and in an external magnetic field of 6 T. The replacement of a quarter of the Fe by Co did not cause significant modifications of the hyperfine interactions in the 57-Fe nuclei. The observed minor variations in the local magnetic microstructure were attributed to alterations in the topological short-range order. However, the in-field 57-Fe Mössbauer spectra indicated a misalignment of the partial magnetic moments. On the other hand, the presence of Co considerably affected the local magnetic microstructure of the 119-Sn nuclei. This was probably due to the higher magnetic moment of Co, which induces transfer fields and polarization effects on the diamagnetic Sn atoms.

Keywords: Mössbauer spectrometry; Fe-57; Sn-119; Fe-based metallic glasses; hyperfine interactions; short-range order

check for updates

Citation: Grey, D.G.; Cesnek, M.; Bujdoš, M.; Miglierini, M.B. Effect of Cobalt on the Microstructure of Fe-B-Sn Amorphous Metallic Alloys. *Metals* **2024**, *14*, 712. https://doi.org/10.3390/met14060712

Academic Editor: Ding Ding

Received: 29 April 2024
Revised: 8 June 2024
Accepted: 14 June 2024
Published: 16 June 2024

Copyright: © 2024 by the authors. Licensee MDPI, Basel, Switzerland. This article is an open access article distributed under the terms and conditions of the Creative Commons Attribution (CC BY) license (https://creativecommons.org/licenses/by/4.0/).

1. Introduction

A material's macroscopic properties are governed by its structure. Thus, the identification of the local atomic arrangement is important for the determination of its behavior and potential applications. The microstructure of materials is sensitive to any external modifications which, consequently, affect their resulting physical properties. From a structural point of view, materials can be classified into two main groups: (i) crystalline materials featuring a long-range order translation symmetry due to a crystallographic arrangement with well-defined atomic positions and (ii) disordered or amorphous materials exhibiting non-equivalent atomic sites, implying that only a short-range order exists in their local atomic arrangement.

The determination of structural positions in materials with an ill-defined structural arrangement results in serious requirements for commonly used characterization techniques. For example, X-ray diffraction performed using small objects provides featureless reflections characteristic of an amorphous structure. The obtained information is very limited and practically of no use. Thus, the characterization of disordered materials represents a challenging task because a significant knowledge gap exists in the determination of their microstructural arrangement. Here, we intend to tackle this problem by employing a detailed analysis of the hyperfine interactions between nuclei and their electron shells, obtained using Mössbauer spectrometry (MS) [1]. Although the resulting spectral lines are

considerably broadened due to the distributions of the corresponding hyperfine parameters, they provide significant information on both the structural and magnetic states of the resonant atoms [2].

The hyperfine interactions can effectively characterize amorphous metallic alloys with a disordered structure. These alloys are also called metallic glasses (MGs) and can contain considerable amounts of iron, which is a key element for MS studies performed upon ^{57}Fe nuclei. Even though these materials were invented several decades ago, they are still attractive to researchers because of their excellent magnetic properties which result in many practical applications, e.g., magnetic shielding, transformers cores, and magnetic sensors [3,4]. Still, the question of their structural arrangement, particularly their structural and/or magnetic transformations, is not yet fully understood.

MGs continue to attract the interest of researchers especially for their excellent soft magnetic properties [5–10]. To enhance their practical applications, both the microstructure and soft magnetic properties of novel MGs are examined, too. Especially, the addition of phosphorus has improved the investigation of parameters. Several new types of P-containing MGs were recently scrutinized [11–14].

Still, novel chemical compositions of Fe-based MGs are designed, aiming at unveiling the role of various elements on their performance. Among them, tin acquires a special position because of its important metallurgical features. It dissolves in solid Fe(Sn) with difficulty and forms practically no solid solution with boron. Recently, the effects of Cu and Co additions on Fe-Sn-B-based MGs were investigated [15–18]. The influence of Sn on the glass forming ability and magnetic properties of Fe-B-P-Sn amorphous alloys with a high Fe content was also reported [19].

Because Sn is the second most widely used isotope in MS, it offers the possibility of scanning the studied materials from two different viewpoints with the help of ^{57}Fe and ^{119}Sn resonant nuclei. There are, however, only a few studies related to Fe-based MGs that also contain Sn [20,21], presumably due to problems with the production of amorphous structures with higher tin contents. ^{119}Sn MS was applied to mechanically alloyed Fe-Sn alloys [22,23], to electrodeposited amorphous alloys [24,25], to amorphous Mn-Sn [26], or to Ni-Mn-Sn metamagnetic alloys [27].

Our motivation in this research is to closely describe the microstructure of Sn-containing Fe-based metallic glasses with the help of hyperfine interactions between the nucleus and the electron shell. In doing so, both ^{57}Fe and ^{119}Sn Mössbauer spectrometry experiments are employed. This study is performed using a Fe-B-Sn MG similar to that reported by Dunlap, who used samples with only a small amount of Sn (up to 2 at. %), because attempts to produce amorphous ribbons with higher Sn contents ($Fe_{75}Sn_5B_{20}$) were (in those days) unsuccessful [20]. Recently, we have investigated MGs with 7 at. % Sn, namely, $Fe_{78}B_{15}Sn_7$ and $Fe_{58.5}Co_{19.5}B_{15}Sn_7$ [15], using ^{57}Fe MS. Here, we extend our research towards ^{119}Sn Mössbauer effect experiments upon the same systems and complement the previous results from ^{57}Fe measurements. In doing so, we have introduced another theoretical model to fit the experimental spectra to distributions of hyperfine magnetic fields. In this way, the results obtained from ^{57}Fe MS reported previously [15] and in this work are complementary.

2. Materials and Methods

Metallic glasses with the nominal composition of $Fe_{78}B_{15}Sn_7$ and $(Fe_3Co_1)_{78}B_{15}Sn_7$ were prepared by the method of planar flow casting at the Institute of Physics, Slovak Academy of Sciences in Bratislava. They were obtained in the form of ribbons approximately 6 mm wide and about 20 μm thick. The actual content of Fe and Co in the investigated samples was determined by flame atomic absorption spectroscopy (F-AAS) using a Perkin-Elmer 1100 spectrometer (PerkinElmer, Inc., Waltham, MA, USA). That of B and Sn was verified with mass spectrometry with inductively coupled plasma (ICP-MS) using a Perkin Elmer Sciex Elan 6000 spectrometer (PerkinElmer, Inc., Waltham, MA, USA).

Mössbauer spectrometry was performed in transmission geometry by employing ^{57}Fe and ^{119}Sn resonant nuclei. For the former, a ^{57}Co/Rh radioactive source was used

whereas the latter experiments were executed with a $^{119m}Sn(CaSnO_3)$ source of gamma radiation; both sources were kept at room temperature. A conventional Wissel spectrometer (WissEl-Wissenschaftliche Elektronik GmbH, Starnberg, Germany) was operated in constant acceleration mode. The calibration of velocity was accomplished using a 12.5 µm thick α-Fe foil for both types of experiments. Isomer shifts obtained from ^{57}Fe and ^{119}Sn experiments are in reference to room-temperature Mössbauer spectra of α-Fe foil and SnO_2, respectively.

Absorbers prepared from as-quenched ribbons were measured at room temperature (RT), 100 K, and 4.2 K. Eventually, an external magnetic field of 6 T oriented parallel to the absorber's plane was applied during the measurements at 4.2 K. During these experiments, the absorbers were placed in a Janis bath cryostat (Janis Research Company, Inc., Woburn, MA, USA). Experiments at 100 K were conducted in a home-made cryostat with a temperature-controlled liquid nitrogen vapor.

Experimental spectra were analyzed using the NORMOS program [28]. Distributions of hyperfine magnetic fields, P(B), were constructed according to the Hesse–Rübartsch histogram method; they were extended over the whole range of possible values of magnetic hyperfine fields, B. They consisted of several sextets (up to 35) with the same line widths taken from the calibration spectrum and the same ratio of line intensities that were, however, fitted in the individual spectra.

3. Results

The amorphousness of the as-quenched ribbons was checked by X-ray diffraction (XRD) as well as by transmission electron microscopy (TEM). Figure 1 shows XRD patterns that are characteristic of completely amorphous samples. The corresponding TEM images can be found elsewhere [15]. These experiments were important specifically to ensure that the production of the MG ribbons yielded an amorphous structure lacking any traces of crystallites, especially when the amount of Sn was close to its solution limit in Fe, which was shown to be up to 9.2 at. % at 1185 K [29]. However, this value was derived from the phase diagrams of binary Fe-Sn systems, while our samples are metastable, and thus, binary phase diagrams do not apply exactly, but can be considered good approximations.

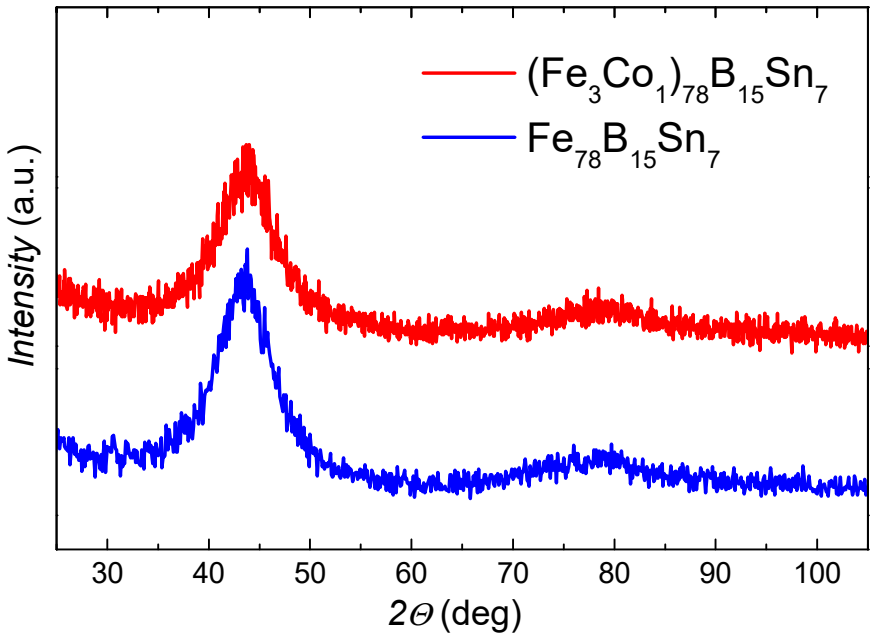

Figure 1. XRD patterns of $Fe_{78}B_{15}Sn_7$ and $(Fe_3Co_1)_{78}B_{15}Sn_7$ MGs in as-quenched state.

Considering this rather severe restriction, it was also necessary to check the actual chemical composition of the investigated MGs, though this aspect is frequently neglected

and only rarely explicitly reported in the literature. The results of the F-AAS and ICP-MS analyses are listed in Table 1.

Table 1. Actual chemical compositions of the investigated samples given in weight (wt.) and atomic (at.) percent (%).

Sample		Fe	Co	B	Sn
$Fe_{78}B_{15}Sn_7$	wt. %	80.0	-	2.85	15.0
	at. %	78.3	-	14.7	7.04
$(Fe_3Co_1)_{78}B_{15}Sn_7$	wt. %	59.6	20.6	2.86	15.0
	at. %	58.6	19.6	14.8	7.06

In the $Fe_{78}B_{15}Sn_7$ MG, only small deviations from the expected nominal composition were detected in Fe (+0.3 at. %) and B (−0.3 at. %). A similar situation has occurred in the $(Fe_3Co_1)_{78}B_{15}Sn_7$ ($Fe_{58.5}Co_{19.5}B_{15}Sn_7$) alloy, where variations in Fe (+0.1 at. %), Co (+0.1 at. %) and B (−0.2 at. %) are also negligible. More importantly, the final content of Sn was, in both MGs, 7 at. %, as required. It is noteworthy that the observed differences in the composition are well below the error range of both analytical methods (~1 wt. %).

3.1. ^{57}Fe Mössbauer Spectrometry

In the evaluation of the spectral parameters, we have introduced a different physical model to fit the calculated theoretical curves to the measured experimental points of the ^{57}Fe Mössbauer spectra, as we have reported in our previous paper [15]. The present concept is similar to that marked as Model I in [21], where a Fe-B-Sn MG containing 5 at. % Sn was studied. Namely, we have employed distributions of hyperfine magnetic fields, P(B). They were reconstructed by a number of individual sextets featuring the same line widths and the same ratios of line intensities corresponding to the individual line pairs, i.e., 1–6, 2–5, and 3–4. The line widths were fixed and their values were taken from the corresponding calibration spectra from the individual experiments. The number of individual sextets varied across separate temperature experiments in such a way that the whole range of expected magnetic hyperfine fields, B, was covered.

The ^{57}Fe Mössbauer spectra of both MGs recorded at RT, 100 K, and 4.2 K are shown in Figure 2 together with their corresponding distributions of hyperfine magnetic fields, P(B). The spectra exhibit characteristic features of ferromagnetic amorphous metallic alloys, i.e., six broad and overlapping, though quite well distinguishable, absorption lines. They also confirm the amorphous structure of the investigated samples as no traces of additional narrow lines, that might indicate the presence of Fe-containing crystalline phases, are observed. Thus, together with the results of the XRD and TEM [15], additional proof of the amorphousness of the produced MGs is provided.

3.2. ^{119}Sn Mössbauer Spectrometry

Mössbauer spectrometry with ^{119}Sn nuclei was performed under the same experimental conditions as the ^{57}Fe ones using the same equipment. Nevertheless, the maximum velocity was substantially enlarged in order to accommodate all the spectra. They are shown for both MGs in Figure 3 along with their P(B) distributions. As can be seen, the shapes of the spectra are notably different from those in Figure 2, showing no obvious six-line patterns. This is caused by low magnetic hyperfine fields that experience the ^{119}Sn resonant nuclei in their nearest neighborhood. As a result, the P(B) distributions extend to smaller B-values than in the case of ^{57}Fe MS experiments and exhibit a considerable probability of the Sn nuclei being in a low-field environment. These results are consistent with those reported elsewhere [20].

Still, in order to evaluate the spectral parameters, we have used the same fitting model as in the previous case of ^{57}Fe experiments with one exception. The ratio of line intensities

of the ^{119}Sn spectra was not free during the fitting procedure. Instead, it was fixed to the value that was taken from the corresponding ^{57}Fe spectra, as suggested by Dunlap [20]. Such an approach assumes similarities in the orientation of the net magnetic moments experienced at ^{57}Fe and ^{119}Sn resonant nuclei inside the same sample.

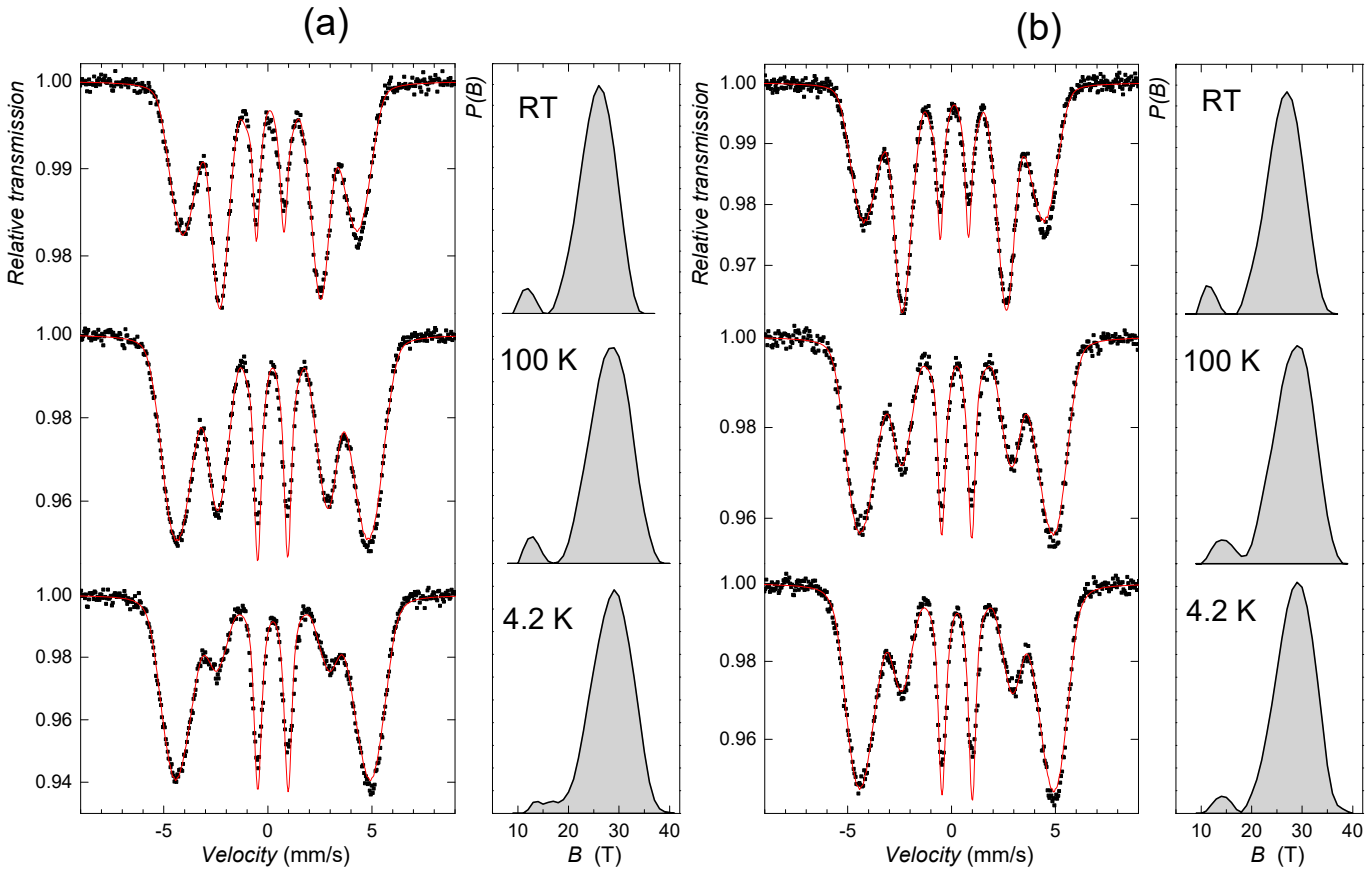

Figure 2. ^{57}Fe Mössbauer spectra (**left-hand panels**) and corresponding distributions of hyperfine magnetic fields, P(B) (**right-hand panels**), of (**a**) $Fe_{78}B_{15}Sn_7$ and (**b**) $(Fe_3Co_1)_{78}B_{15}Sn_7$ MGs recorded at the indicated temperatures.

3.3. External Magnetic Field

In order to analyze the magnetic microstructure of the investigated MGs in more detail, we have also performed the low-temperature (4.2 K) experiments in an external magnetic field of 6 T that was oriented parallel to the plane of the absorber. The obtained ^{57}Fe and ^{119}Sn Mössbauer spectra are depicted in Figures 4 and 5, respectively, together with the corresponding distributions of hyperfine magnetic fields, P(B).

The spectral parameters obtained from all the experiments comprising average values of hyperfine magnetic fields, <B>, isomer shifts, <δ>, and values of Θ angles are listed in Table 2. The corresponding errors in the determination of <δ> and Θ are ±0.02 mm/s and ±1.5°, respectively. Those of <B> are ±0.3 T and ±0.05 T for the ^{57}Fe and ^{119}Sn experiments, respectively. As mentioned above, the positions of the magnetic moments in the ^{119}Sn spectra were considered equal to those in the ^{57}Fe spectra; hence, the values of the Θ angles apply to both the ^{57}Fe and ^{119}Sn Mössbauer effect experiments.

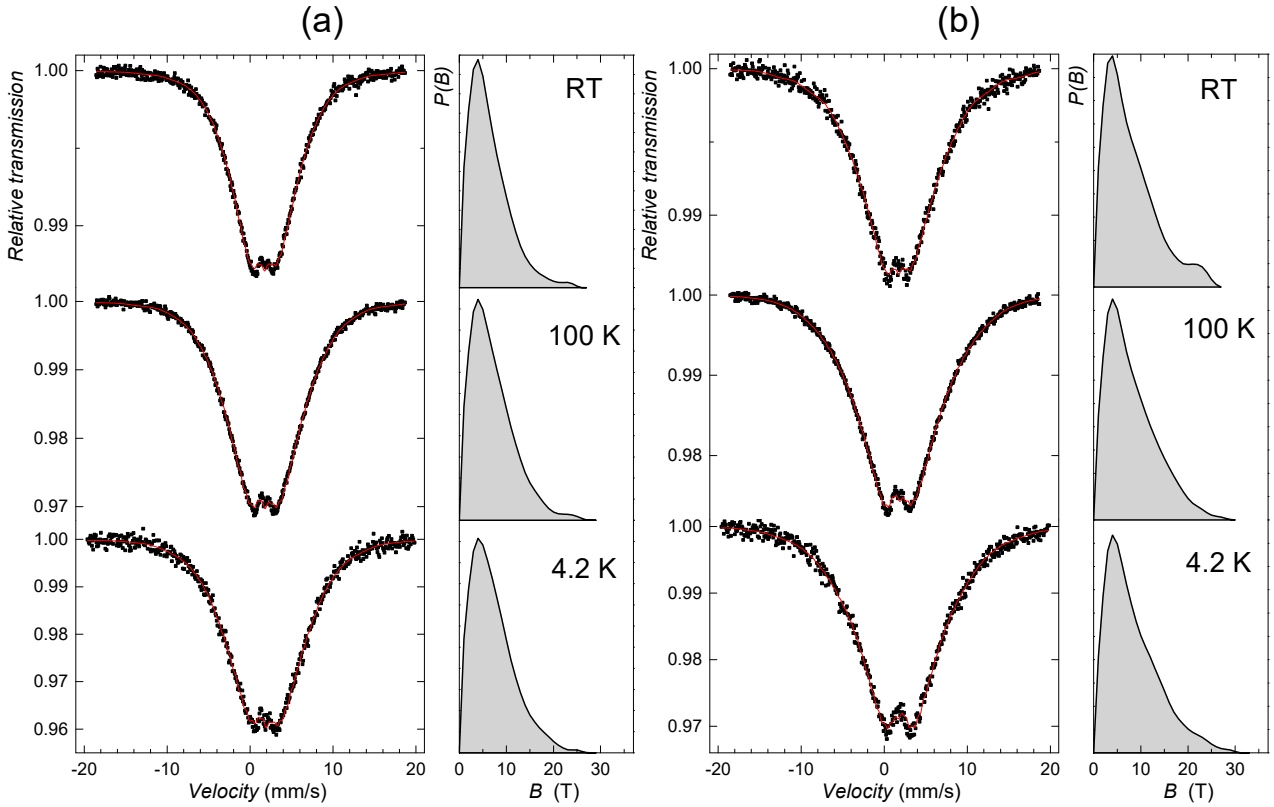

Figure 3. ^{119}Sn Mössbauer spectra (**left-hand panels**) and corresponding distributions of hyperfine magnetic fields, P(B) (**right-hand panels**), of (**a**) $Fe_{78}B_{15}Sn_7$ and (**b**) $(Fe_3Co_1)_{78}B_{15}Sn_7$ MGs recorded at the indicated temperatures.

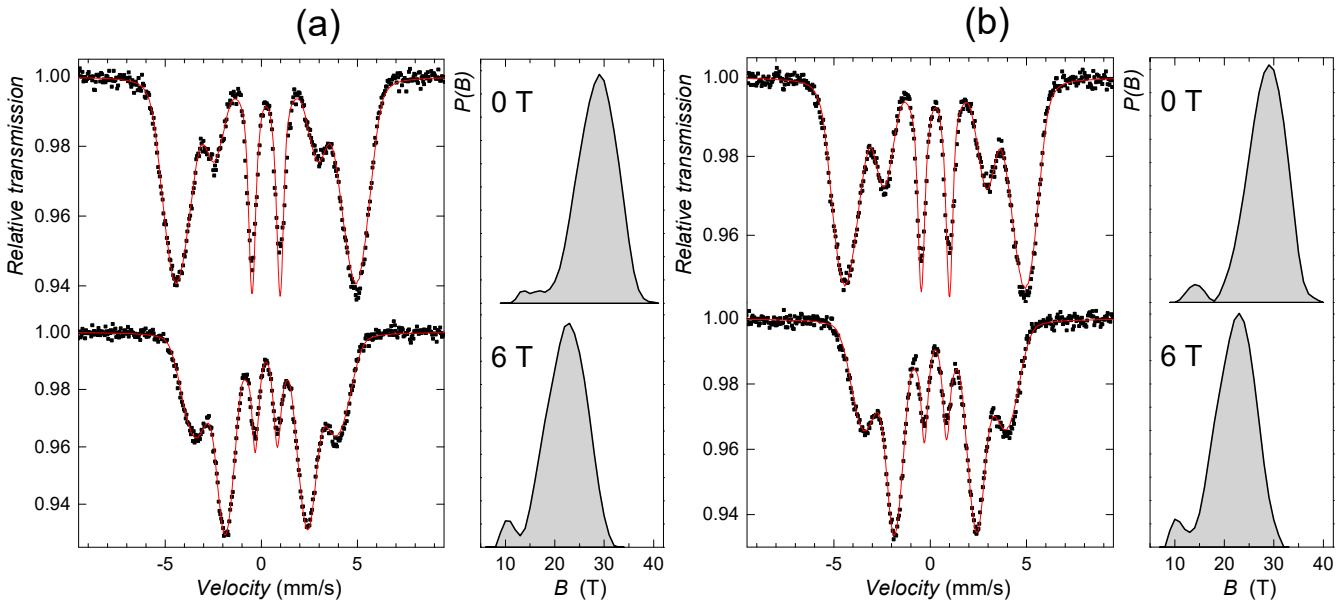

Figure 4. ^{57}Fe Mössbauer spectra (**left-hand panels**) and corresponding distributions of hyperfine magnetic fields, P(B) (**right-hand panels**) of (**a**) $Fe_{78}B_{15}Sn_7$ and **(b)** $(Fe_3Co_1)_{78}B_{15}Sn_7$ MGs recorded at 4.2 K without and with an external magnetic field of 6 T.

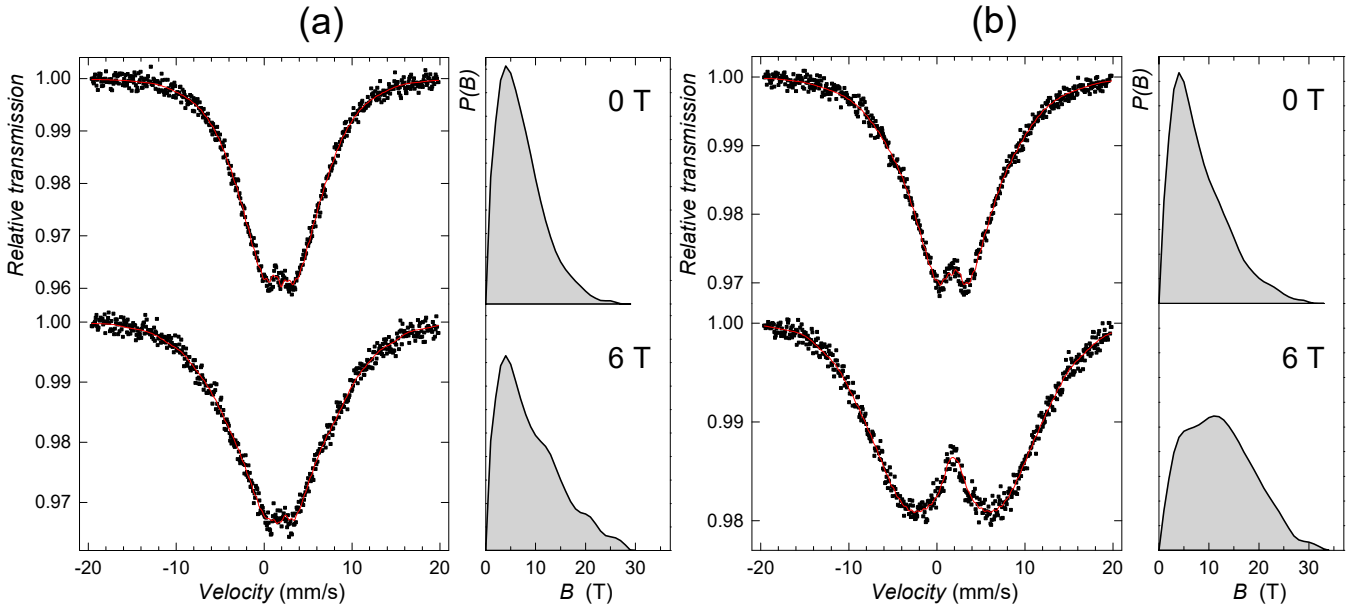

Figure 5. ^{119}Sn Mössbauer spectra (**left-hand panels**) and corresponding distributions of hyperfine magnetic fields, P(B) (**right-hand panels**), of (**a**) $Fe_{78}B_{15}Sn_7$ and (**b**) $(Fe_3Co_1)_{78}B_{15}Sn_7$ MGs recorded at 4.2 K without and with an external magnetic field of 6 T.

Table 2. Parameters of ^{57}Fe and ^{119}Sn Mössbauer spectra of the as-quenched MGs taken under the specified conditions.

Sample	Condition	Parameters				
		Θ (deg)	^{57}Fe MS		^{119}Sn MS	
			<B> (T)	<δ> (mm/s)	<B> (T)	<δ> (mm/s)
$Fe_{78}B_{15}Sn_7$	RT	65.8	25.2	0.11	5.50	1.74
	100 K	48.1	27.5	0.25	6.11	1.76
	4.2 K	31.2	28.2	0.25	6.20	1.79
	4.2 K/6 T	77.3	22.0	0.24	8.04	1.67
$(Fe_3Co_1)_{78}B_{15}Sn_7$	RT	70.2	26.0	0.13	6.86	1.75
	100 K	41.9	27.8	0.26	7.09	1.76
	4.2 K	37.1	28.1	0.26	7.37	1.80
	4.2 K/6 T	78.4	22.0	0.26	11.26	1.93

4. Discussion

A bimodal nature of the hyperfine magnetic field distributions, P(B), which can be seen in Figure 2, is frequently observed in these types of ^{57}Fe Mössbauer spectra and features the so-called low- and high-field humps. Because a discussion about the origin of this bimodal behavior is beyond the scope of this paper, we provide only average values of the P(B) distributions, <B>, as they do not substantially depend (within the error range) upon the evaluation model used. A visualization of all the spectral parameters is presented in Figure 6; those corresponding to the $Fe_{78}B_{15}Sn_7$ MG are plotted as blue (^{57}Fe experiments) and dark cyan (^{119}Sn) solid circles while those of the $(Fe_3Co_1)_{78}B_{15}Sn_7$ MG are given by the same symbols in red (^{57}Fe) and magenta (^{119}Sn). The spectral parameters obtained from the in-field (6 T) spectra at 4.2 K use the same color coding but are plotted as solid squares. Error bars are also provided; those that are not visible are smaller than the sizes of the respective symbols. The solid lines are only guides for the eye; the dashed green line in

Figure 6a represents Θ = 54.7°. As already mentioned, the Θ angle is considered equal for both MGs and that is why only the data from the ^{57}Fe Mössbauer effect experiments are shown in Figure 6a.

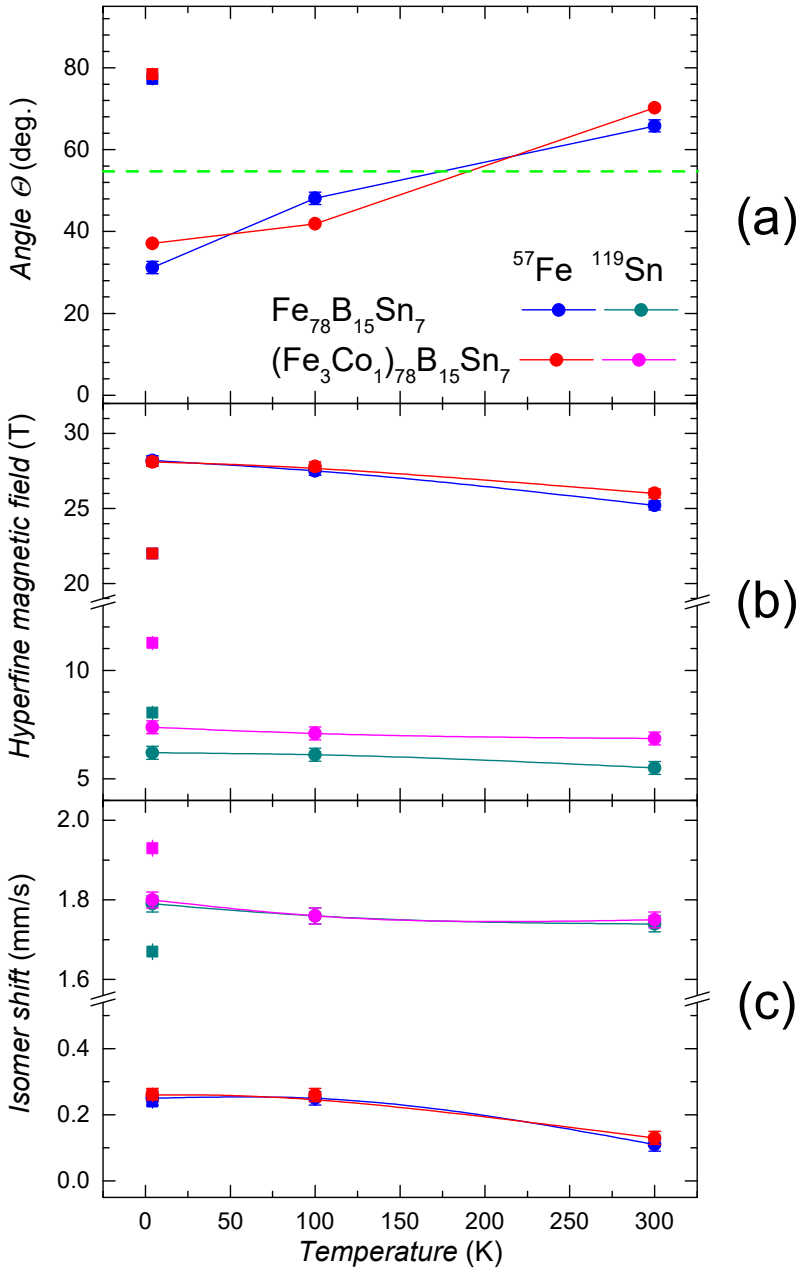

Figure 6. Parameters of ^{57}Fe and ^{119}Sn Mössbauer spectra of $Fe_{78}B_{15}Sn_7$ and $(Fe_3Co_1)_{78}B_{15}Sn_7$ MGs as a function of temperature of measurement: (**a**) Position of the net magnetization characterized by an angle Θ, (**b**) average hyperfine magnetic field, and (**c**) average isomer shift. An explanation of the symbols is provided in the text.

Looking at the ^{57}Fe Mössbauer spectra in Figure 2 and taking into account their respective spectral parameters (see Table 2 and Figure 6), the following observations can be made. When decreasing the temperature of the measurements, the <B>-values increase and so do the <δ>-values. Both trends are in accordance with the temperature behavior of these parameters, as expected. On the other hand, a comparison of <B> derived from the $Fe_{78}B_{15}Sn_7$ MG with those where 25% of the Fe atoms were replaced by Co, i.e., $(Fe_3Co_1)_{78}B_{15}Sn_7$, shows only a moderate increase of ~0.8 T. Also, assuming practically no

change in the <δ>-value within the error range after inserting Co into the basic composition, one can conclude that this increase in <B> is not caused by the modification of the chemical short-range order (SRO). Instead, variations in the topological SRO should be considered. They reflect the structural rearrangement of the constituent atoms and/or changes in their magnetic states. This also affects the positions of the spins, which is demonstrated by a monotonous change in the Θ angles with a decreasing temperature of measurement.

The Mössbauer spectra obtained from the ^{119}Sn experiments, which are shown in Figure 3, exhibit rather featureless line shapes. Similar spectra were reported by Dunlap [20] for a $Fe_{80-x}Sn_xB_{20}$ amorphous ferromagnet. Contrary to the ^{57}Fe spectra in Figure 2, they extend over at least twice as large a velocity range. On the other hand, the associated P(B) distributions show significant probability values in the low-field regions (up to ~10 T). This might be caused by a mutual cancelation of large negative contributions to the hyperfine field of the Sn atoms by their nearest neighborhoods with a more positive one stemming from remote neighborhoods, similar to what is observed in ordered bcc systems [30].

The magnetic microstructure of the sample affects the rotation of spins that establish the net magnetization (the net magnetic moment) of the sample; the Θ angle is related to this position. In the case of Θ = 90°, the individual magnetic moments of the resonant atoms are located within the plane of the absorber (sample), while Θ = 0° indicates their perpendicular orientation. The random positions of the magnetic moments that are found, e.g., in powder samples, are characterized by the so-called magic angle of Θ = 54.7° (green dashed line in Figure 6a).

Namely, at a low temperature, the spins freeze in more favorable positions. It should be noted that with decreasing temperature, the net magnetic moments of both MGs progressively turned out from their original positions at RT towards a more pronounced out-of-plane direction, as evidenced by a decrease in the Θ angles in Figure 6a. This rotation amounts to almost ~18° and 35° in $Fe_{78}B_{15}Sn_7$ and about 28° and 33° in the Co-containing MGs during the temperature drop down to 100 K and 4.2 K, correspondingly. This massive movement of spins is reflected by a dramatic decrease in the line intensities of the second and fifth Mössbauer lines, as documented in Figure 2.

Due to the ferromagnetic nature of the investigated samples, we can conclude that the replacement of Fe by Co does not substantially affect the magnetic microstructure of amorphous $(Fe_3Co_1)_{78}B_{15}Sn_7$ in comparison with the Co-free $Fe_{78}B_{15}Sn_7$ MG. Only minor alternations in the local neighborhood of the ^{57}Fe resonant nuclei with the consequent rearrangement of the topological SRO are evidenced by a rather small increase in the <B>- and Θ-values at RT, yielding relative changes in the respective spectral parameters of ~3% and less than 7%. Changes in <δ> are within the experimental error.

These relatively small deviations in <B> and Θ after the incorporation of Co into the basic composition of the Fe-B-Sn alloy were almost eliminated when the ^{57}Fe experiments were performed at 4.2 K in an external magnetic field of 6 T oriented parallel to the plane of the absorber. As a result, the relative differences between these two types of MGs are smaller than 1% and only slightly higher than 1%, correspondingly.

The reported <B>-values derived from the in-field experiments represent effective magnetic fields that locally act upon the resonant atoms. They result from the mutual interaction of the internal hyperfine magnetic field at the particular nuclei and the external one. Consequently, depending upon the magnetic microstructure, the measured effective field can be lowered (or enhanced) by as much as the magnetic induction of the external magnetic field (6 T in our case) is. Indeed, when comparing the in-field experiments with those performed in the zero field at 4.2 K, the in-field measurements yielded <B>-values for $Fe_{78}B_{15}Sn_7$ and $(Fe_3Co_1)_{78}B_{15}Sn_7$ that were smaller by 6.20 T and 6.16 T, respectively. The P(B) distributions corresponding to the ^{57}Fe Mössbauer spectra in Figure 4 are notably shifted towards low hyperfine magnetic fields when a 6 T external field is applied. This is caused by a negative field at the nuclei of the Fe atoms in metallic Fe [31], which presumably acts likewise in Fe-based amorphous alloys.

Apart from the effective hyperfine field, the external magnetic field also affects the individual magnetic moments of the resonant atoms and, consequently, the position of the net magnetization (angle Θ). Because the external magnetic field is oriented parallel to the plane of the absorber (sample), it is supposed to rotate the spins into the in-plane positions, at Θ = 90°. Indeed, this tendency is clearly seen in the Mössbauer spectra of both samples in Figure 4 by a notable increase in the intensities of their second and fifth spectral lines when the external field is applied. Nevertheless, despite the fact that the net magnetic moments for the $Fe_{78}B_{15}Sn_7$ and $(Fe_3Co_1)_{78}B_{15}Sn_7$ MGs have moved towards the absorber's plane by more than 46° and 41° with respect to the zero-field experiments, respectively, their final locations are far from being completely oriented within the plane of the samples. In fact, a difference of nearly 13° and 12°, respectively, is detected. This observation indicates that magnetic regions exist in the investigated samples where the spins are dominantly oriented in the out-of-plane direction.

The electronic structure in the local environments of the resonant atoms is reflected by the measured isomer shift. Nevertheless, no changes in <δ> are observed in the ^{57}Fe Mössbauer spectra of either samples when an external magnetic field is applied. As mentioned above, the <B>-values of the in-field ^{57}Fe spectra measured at 6 T exhibit differences of ~0.2 T from the theoretically feasible values. This suggests that variations in the magnetic microstructure should be considered. It is noteworthy that the observed differences in <B> are of a comparable value in both MGs regardless of their chemical compositions, which were, eventually, modified by Co addition. This is another factor in support of our hypothesis that deviations in the chemical SRO are not responsible for the observed modifications of the magnetic microstructure at the ^{57}Fe sites of the as-quenched MGs.

Similarly, in the case of the ^{57}Fe nuclei, the average hyperfine magnetic fields of the ^{119}Sn atoms, <B>, also increase with decreasing temperature and so do the average isomer shifts, <δ> (Table 2, Figure 6). It is, however, noteworthy that, unlike in the ^{57}Fe Mössbauer spectra, where the <B>-values of the Co-free and Co-containing MGs are very close to each other over the whole temperature range, the <B> obtained from the ^{119}Sn experiments with the Co-containing amorphous alloy exhibit systematically higher values, by ca. 1.2 T (~20%) on average, which is well above the experimental error. As for the <δ>-values, they are identical within the error range over all the temperatures and behave similarly as those of the ^{57}Fe nuclei. Thus, a conclusion can be made that no appreciable deviations in the chemical SRO are encountered, instead, modifications of the topological SRO should be considered that affect the <B>-values.

The application of an external magnetic field has introduced even more pronounced differences in the <B>-values of the ^{119}Sn nuclei. They are ~23% higher in the Co-free sample with respect to the zero-field experiment and by ~35% in the Co-containing sample. Such an enormous increase in the <B> at the ^{119}Sn nuclei, especially for the Co-containing MG, is obvious also from the shapes of the Mössbauer spectra and their P(B) distributions in Figure 5. In particular, the latter notably extend towards higher <B>-values.

In ordered FeCo, Sn atoms are supposed to preferentially enter the Co sites where they exhibit larger hyperfine fields [32]. They are manifested by the appearance of more pronounced high-field tails in the P(B) distributions, corresponding to the Co-containing MG in Figure 5, as well as a notable increase in the probability values close to 15 T. This might be an indication of a dominant positive contribution to the hyperfine magnetic field at the Sn sites [20], which might be further enhanced by the so-called transferred hyperfine fields at the ^{119}Sn nuclei due to small or even neglecting the Co magnetic moment [33]. In addition, a higher accumulation of Fe atoms, especially in more distant surroundings of the Sn nuclei, is also probable. In an ordered system, contributions to the hyperfine magnetic field from the nearest neighborhoods (the first coordination sphere) and those from more distant atoms in the second coordination sphere are considered additive and proportional to the magnetic moments of each region [30]. The same concept was also introduced for the case of the Fe-Sn-B amorphous system [20]. Thus, the P(B) distributions at the Sn sites

reflect influences stemming from positive and negative contributions to the spin density at the Sn nuclei from the Fe nearest neighbors. This assumption is underlined by the fact that Sn is more soluble in Fe than in Co [32]. Finally, the more pronounced increase in the <B> might be caused by the fact that the Sn may introduce strong antiferromagnetic coupling between its Co neighbors in addition to an overlap of the 5s orbital in Sn with that of 3d in Co [34].

Contrary to the development of the <δ>-values in the external magnetic field applied in the ^{57}Fe MS experiments, which are almost unchanged (see Figure 6c), the ^{119}Sn measurements show notable deviations in <δ> in comparison with the zero-field ones. In addition, in the Co-free sample, the observed differences are towards (notably) lower <δ>-values, whereas the opposite trend was revealed for the $(Fe_3Co_1)_{78}B_{15}Sn_7$ MG. As a change in the s-electron density of a nucleus will initiate a change in the corresponding isomer shift values [1], the polarization of the 3d electrons in the surrounding atoms (Fe and/or Co in our case) may cause a change in the relative spatial distribution of the 4s electrons in the Sn atoms [35].

5. Conclusions

The microstructure of the $Fe_{78}B_{15}Sn_7$ and $(Fe_3Co_1)_{78}B_{15}Sn_7$ metallic glasses was investigated by employing ^{57}Fe and ^{119}Sn Mössbauer spectrometry. The impact of Co substitution for Fe atoms was determined by using the hyperfine interactions between the resonant nuclei and their electron shells.

As evidenced by the results of the ^{57}Fe experiments, the replacement of one quarter of the Fe atoms with Co in the original composition did not impose significant changes in the spectral parameters derived from the measured spectra. The observed deviations in the hyperfine interactions at the ^{57}Fe resonant nuclei follow this expected (and rather predictable) tendency. They point out only minor deviations in the local magnetic microstructure, which are related to small changes in the topological short-range order due to the presence of Co. Because no appreciable changes were revealed in the isomer shift values, modifications of the chemical short-range order can be excluded.

An important finding from the ^{57}Fe in-field Mössbauer experiments is that not all partial magnetic moments in the investigated samples are aligned in the direction of the external magnetic field. This is documented by the Θ angles that do not reach 90°. Consequently, there should be magnetic regions in the investigated samples where the spins are dominantly oriented in the out-of-plane direction. That might be due to the magnetic environments of the Fe nuclei that are influenced by the presence of possible magnetic vacancies. This conclusion holds for both Co-free and Co-containing MGs, meaning that the impact of the higher magnetic moment of the Co atoms does not play a significant role.

The application of ^{119}Sn Mössbauer spectrometry leads to the following conclusions: The striking differences in the shapes of the ^{57}Fe and ^{119}Sn Mössbauer spectra are on account of the much lower local hyperfine magnetic fields at the latter nuclei. On average, they are reduced by ~21 T and ~20 T in the samples without and with Co, respectively, as derived from zero-field Mössbauer spectra. The in-field spectra exhibit corresponding differences of ~14 T and ~11 T. In addition, the <B>-values obtained from the zero-field ^{119}Sn Mössbauer spectra of the alloy with Co are systematically higher by about 1.2 T in comparison with those derived from the Co-free metallic glass.

All these findings allow us to conclude that the presence of Co considerably affects the local magnetic microstructure, as proven by the ^{119}Sn nuclei. The reason for this may originate from differences in the magnetic moments of Fe and Co and their impact via transferred fields and polarization effects upon diamagnetic Sn atoms. Specifically, the polarization effects might be responsible for rather big modifications of the isomer shifts obtained from the in-field experiments that are, moreover, of an opposite sign for the investigated Co-free and Co-containing Fe-(Co)-B-Sn metallic glass.

Finally, we would like to note that despite the extensive content of Sn in the studied alloys (7 at. %), which is close to the solubility limit of Sn in the Fe matrix, the samples

were fully amorphous and no traces of crystalline phases were detected. The obtained results can contribute to the design of novel types of MGs with suitable soft magnetic properties, which are important for industrial applications. They are potential alternatives to the 'classical' compositions of nanocrystalline alloys like NANOPERM, HITPERM, or even NANOMET and can ensure the sustainability of soft amorphous magnetic material production at reasonable costs. Moreover, the studied Fe(Co)-B-Sn MGs exhibit a nanocrystalline structure after appropriate heat treatment [17], which ultimately leads to the desired soft magnetic properties.

Author Contributions: D.G.G.: formal analysis, investigation, writing—original draft; M.C.: data curation, investigation, validation, visualization; M.B.: formal analysis, investigation, visualization, M.B.M.: conceptualization, funding acquisition, methodology, project administration, writing—review and editing. All authors have read and agreed to the published version of the manuscript.

Funding: This work was supported by the Scientific Grant Agency of the Ministry of Education, Science, Research and Sport of the Slovak Republic: VEGA 1/0010/24, by the European Regional Development Fund-Project "Centre for Advanced Applied Sciences": CZ.02.1.01/0.0/0.0/16_019/0000778, and the Large Research Infrastructures of the Ministry of Education, Youth and Sports of the Czech Republic: LM2023073.

Data Availability Statement: The raw data supporting the conclusions of this article will be made available by the authors on request.

Acknowledgments: As-quenched metallic glasses were received by a courtesy of P. Švec from the Institute of Physics, Slovak Academy of Sciences in Bratislava.

Conflicts of Interest: The authors declare no conflicts of interest.

References

1. Nasu, S. General Introduction to Mössbauer Spectroscopy. In *Mössbauer Spectroscopy*, 1st ed.; Yoshida, Y., Langouche, G., Eds.; Springer: Berlin/Heidelberg, Germany, 2013; pp. 1–22. [CrossRef]
2. Miglierini, M.; Matúš, P. Structural modifications of metallic glasses followed by techniques of nuclear resonances. *Pure Appl. Chem.* **2017**, *89*, 405–417. [CrossRef]
3. Herzer, G. Modern soft magnets: Amorphous and nanocrystalline materials. *Acta Mater.* **2013**, *61*, 718–734. [CrossRef]
4. Jez, B.; Postawa, P.; Nabiałek, M. Structure and properties of magnetic composites based on amorphous Fe alloys. *Bul. Pol. Acad. Sci.* **2023**, *71*, e144608. [CrossRef]
5. Yang, Z.Z.; Zhu, L.; Jiang, S.S.; Zhu, C.; Xu, Q.H.; Lin, Y.; Chen, F.G.; Wang, Y.G. Nanoscale structural heterogeneity and magnetic properties of Fe-based amorphous alloys via Co and Ni additions. *J. Alloys Compd.* **2022**, *904*, 164067. [CrossRef]
6. Panahi, S.L.; Garcia-Ramón, M.; Pineda, E.; Bruna, P. New (FeCoCrNi)-(B,Si) high-entropy metallic glasses, study of the crystallization processes by X-ray diffraction and Mössbauer spectroscopy. *J. Non-Cryst. Solids* **2020**, *547*, 120301. [CrossRef]
7. Li, T.; Li, Y.; Wu, L.; Qi, L.; Zhang, W. Improvement of soft magnetic properties of a $Fe_{84}Nb_7B_9$ nanocrystalline alloy by synergistic substitution of P and Hf. *J. Alloys Compd.* **2022**, *918*, 165735. [CrossRef]
8. Yang, Z.Z.; Jiang, S.S.; Ye, L.X.; Zhu, C.; Gao, X.; Yang, H.; Wang, Y.G. Nanoscale structural heterogeneity perspective on the ameliorated magnetic properties of a Fe-based amorphous alloy with decreasing cooling rate. *J. Non-Cryst. Solids* **2022**, *581*, 121433. [CrossRef]
9. Sünbül, S.E.; Akyol, S.; İçin, K.; Umićević, A.; Ivanovski, V.; Batalović, K. Investigating oxidation behavior of $Fe_{38}Co_{38}Mo_8B_{15}Cu_1$ alloy ribbons—Structural, magnetic and Mössbauer study. *J. Non-Cryst. Solids* **2024**, *627*, 122836. [CrossRef]
10. Zamora, J.; Betancourt, I.; García Hinojosa, J.A. The Influence of Boron on Microstructural Evolution, Mechanical and Magnetic Behavior of Amorphous $Fe_{91-x}Zr_5Nb_4B_x$ Melt-Spun Alloys. *Metals* **2022**, *12*, 994. [CrossRef]
11. Xu, T.; Yao, J.; Zhuo, L.; Jie, Z. Tuning Non-Isothermal Crystallization Kinetics between $Fe_{20}Co_{20}Ni_{20}Cr_{20}(P_{0.45}B_{0.2}C_{0.35})_{20}$ High-Entropy Metallic Glass and the Predecessor $Fe_{75}Cr_5P_9B_4C_7$ Metallic Glass. *Metals* **2023**, *13*, 1624. [CrossRef]
12. Huang, X.; Ding, S.; Wang, Z.; Wang, L.; Liu, M.; Wang, Z.; Liang, X.; Liu, W. Effects of annealing temperature on the structure characteristics of $Fe_{83}Si_6B_6Cu_1Nb_1P_{1.5}C_{1.5}$ amorphous ribbons. *J. Non-Cryst. Solids* **2022**, *580*, 121388. [CrossRef]
13. Zhang, H.; Bai, F.; Dong, Y.; Xie, L.; Li, Q.; He, A.; Li, J. Effect of Ge Addition on Magnetic Properties and Crystallization Mechanism of FeSiBPNbCu Nanocrystalline Alloy with High Fe Content. *Metals* **2022**, *12*, 640. [CrossRef]
14. Butvinová, B.; Švec Sr., P.; Janotová, I.G.; Dias, L.V.; Janičkovič, D.; Maťko, I. Magnetic properties and structure of short-term annealed FeCuBPSi nanocrystalline alloys. *J. Magn. Magn. Mater.* **2024**, *590*, 171662. [CrossRef]
15. Miglierini, M.B.; Dekan, J.; Cesnek, M.; Janotová, I.; Švec, P.; Bujdoš, M.; Kohout, J. Hyperfine interactions in Fe/Co-B-Sn amorphous alloys by Mössbauer spectrometry. *J. Magn. Magn. Mater.* **2020**, *500*, 166417. [CrossRef]

16. Butvinová, B.; Švec Sr., P.; Janotová, I.; Fos, A.; Maťko, I.; Janičkovič, D. Magnetic and structural properties of $(Fe\text{-}Co)_{83}(Sn\text{-}P)_5B_{12}$ alloys with high saturation. *J. Magn. Magn. Mater.* **2021**, *535*, 168069. [CrossRef]
17. Fos, A.; Švec Sr., P.; Janotová, I.; Janičkovič, D.; Butvinová, B.; Búran, M.; Kyritsi, A.; Konstantinidis, N.; Novák, P. Effect of Cu and Co addition on non-isothermal crystallization kinetics of rapidly quenched Fe-Sn-B based alloys. *J. Non-Cryst. Solids* **2022**, *593*, 121785. [CrossRef]
18. Maťko, I.; Illeková, E.; Švec Sr., P.; Švec, P.; Janičkovič, D.; Vodárek, V. Microstructural study of the crystallization of amorphous Fe–Sn–B ribbons. *J. Alloys Compd.* **2014**, *615*, S462–S466. [CrossRef]
19. Li, X.; Liu, J.; Qu, C.; Song, K.; Hu, L.; Wang, L. Preparation and properties of Fe-B-P-Sn soft magnetic amorphous alloys with Fe contents higher than 83%. *J. Non-Cryst. Solids* **2017**, *469*, 27–30. [CrossRef]
20. Dunlap, R.A. Sn and Fe hyperfine field distributions in the amorphous ferromagnet $Fe_{80-x}Sn_xB_{20}$. *Solid State Commun.* **1982**, *43*, 57–60. [CrossRef]
21. Miglierini, M.; Rusakov, V.S. ^{57}Fe and ^{119}Sn Mössbauer Effect Study of Fe-Sn-B Amorphous Alloys. *AIP Conf. Proc.* **2010**, *1258*, 29–38. [CrossRef]
22. Costa, B.F.O.; Le Caër, G.; Amado, M.M.; Sousa, J.B.; Ayres de Campos, N. Magnetic properties of coarse-grained and nanocrystalline Fe–Cr–Sn alloys. *J. Alloys Compd.* **2000**, *308*, 49–55. [CrossRef]
23. Yelsukov, E.P.; Voronina, E.V.; Konygin, G.N.; Barinov, V.A.; Godovikov, S.K.; Dorofeev, G.A.; Zagainov, A.V. Structure and magnetic properties of $Fe_{100-x}Sn_x$ ($3.2 < x < 62$) alloys obtained by mechanical milling. *J. Magn. Magn. Mater.* **1997**, *166*, 334–348. [CrossRef]
24. Kuzmann, E.; Sziráki, L.; Stichleutner, S.; Homonnay, Z.; Lak, G.B.; El-Sharif, M.; Chisholm, C.U. Mössbauer and XRD study of novel quaternary Sn-Fe-Co-Ni electroplated alloy. *Hyperfine Int.* **2017**, *238*, 97. [CrossRef]
25. Stichleuter, S.; Lak, G.B.; Kuzmann, E.; Chisholm, C.U.; El-Sharif, M.; Homonnay, Z.; Sziráki, L. Mössbauer and XRD study of pulse plated Sn-Fe, Sn-Ni and Sn-Ni-Fe electrodeposited alloys. *Hyperfine Int.* **2014**, *226*, 15–25. [CrossRef]
26. Drago, V.; Baggio Saitovitch, E. Short range order in vapor quenched amorphous Mn_xSn_{1-x} alloys using in situ ^{119}Sn Mössbauer spectroscopy. *Solid State Commun.* **1987**, *64*, 153–155. [CrossRef]
27. Unzueta, I.; López-García, J.; Sánchez-Alarcos, V.; Recarte, V.; Pérez-Landazábal, J.I.; Rodríguez-Velamazán, J.A.; Garitaonandia, J.S.; García, J.A.; Plazaola, F. Testing the Applicability of ^{119}Sn Mössbauer Spectroscopy for the Internal Stress Study in Ternary and Co-Doped Ni-Mn-Sn Metamagnetic Alloys. *Metals* **2021**, *11*, 450. [CrossRef]
28. Brand, R.A. Improving the validity of hyperfine field distributions from magnetic alloys: Part I: Unpolarized source. *Nucl. Instrum. Methods Phys. Res. B Beam Interact. Mater. At.* **1987**, *28*, 398–416. [CrossRef]
29. Giefers, H.; Nicol, M. High pressure X-ray diffraction study of all Fe-Sn intermetallic compounds and one Fe-Sn solid solution. *J. Alloys Compd.* **2006**, *422*, 132–144. [CrossRef]
30. Delyagin, N.N.; Kornienko, E.N. Magnetic hyperfine interaction for tin atoms in metallic ferro- and antiferromagnets with bcc structure. *Sov. Phys. JETP* **1972**, *34*, 1036–1041.
31. Balabanov, A.E.; Delyagin, N.N. Temperature dependence of the magnetic hyperfine interaction for impurity atoms in metallic ferromagnets. *Sov. Phys. JETP* **1970**, *30*, 1054–1058.
32. Huffman, G.P.; Dunmyre, G.R. Hyperfine fields at ^{119}Sn nuclei in ordered Fe-Co and γ-Fe-Mn. *AIP Conf. Proc.* **1973**, *10*, 1361–1364. [CrossRef]
33. Kulshreshtha, S.K.; Raj, P. Transferred hyperfine fields at ^{119}Sn in $Fe_{1-x}M_xSn$ [*M* = Mn, Co and Ni]. *Solid State Commun.* **1978**, *28*, 787–791. [CrossRef]
34. Jain, A.P.; Cranshaw, T.E. Anomalous temperature dependence of the hyperfine fields at Sn in cobalt. *Phys. Lett. A* **1967**, *25*, 421–422. [CrossRef]
35. Boyle, A.J.F.; Bunbury, D.S.P.; Edwards, C. Polarization of the conduction electrons in the ferromagnetic metals. *Phys. Rev. Lett.* **1960**, *5*, 553–556. [CrossRef]

Disclaimer/Publisher's Note: The statements, opinions and data contained in all publications are solely those of the individual author(s) and contributor(s) and not of MDPI and/or the editor(s). MDPI and/or the editor(s) disclaim responsibility for any injury to people or property resulting from any ideas, methods, instructions or products referred to in the content.